Nucleus basalis-enabled stimulus-specific plasticity in the visual cortex is mediated by astrocytes

Naiyan Chen[a,1], Hiroki Sugihara[a,1], Jitendra Sharma[a,b], Gertrudis Perea[a], Jeremy Petravicz[a], Chuong Le[a], and Mriganka Sur[a,2]

[a]Picower Institute for Learning and Memory, Department of Brain and Cognitive Sciences, Massachusetts Institute of Technology, Cambridge, MA 02139; and [b]Athinoula A. Martinos Center for Biomedical Imaging, Massachusetts General Hospital, Charlestown, MA 02129

Edited by Richard L. Huganir, The Johns Hopkins University School of Medicine, Baltimore, MD, and approved August 31, 2012 (received for review April 18, 2012)

Although cholinergic innervation of the cortex by the nucleus basalis (NB) is known to modulate cortical neuronal responses and instruct cortical plasticity, little is known about the underlying cellular mechanisms. Using cell-attached recordings in vivo, we demonstrate that electrical stimulation of the NB, paired with visual stimulation, can induce significant potentiation of visual responses in excitatory neurons of the primary visual cortex in mice. We further show with in vivo two-photon calcium imaging, ex vivo calcium imaging, and whole-cell recordings that this pairing-induced potentiation is mediated by direct cholinergic activation of primary visual cortex astrocytes via muscarinic AChRs. The potentiation is absent in conditional inositol 1,4,5 trisphosphate receptor type 2 KO mice, which lack astrocyte calcium activation, and is stimulus-specific, because pairing NB stimulation with a specific visual orientation reveals a highly selective potentiation of responses to the paired orientation compared with unpaired orientations. Collectively, these findings reveal a unique and surprising role for astrocytes in NB-induced stimulus-specific plasticity in the cerebral cortex.

acetylcholine | response potentiation | glial calcium | basal forebrain | astrocyte-neuron interactions

Sensory experience associated with nucleus basalis (NB)-driven, cholinergic activation of the cortex (1) has been shown to induce cortical plasticity at both single-cell and cortical map levels (2–6). To understand how cortical responses and representations can be altered by experience during cholinergic modulation, it is critical to identify the circuit elements involved and define how their interactions can contribute to the restructuring of cortical network dynamics.

Previous studies have shown that multiple cortical cell types, including neurons (7–9) and astrocytes (10–12), can be responsive to ACh. Among these cell types, astrocytes are a promising candidate for contributing to NB-mediated cortical plasticity. Ex vivo studies have implicated hippocampal astrocytes in synaptic potentiation [(13–15) compare with (16)], demonstrating that they can potentially provide a powerful means of altering the state of neuronal networks to induce plasticity. More recently, studies using combined somatosensory and cholinergic stimulation have revealed that NB-induced astrocytic activation can induce potentiation of local field potentials recorded in somatosensory cortex (17, 18). These findings open up several key questions. Does the NB-mediated potentiation manifest at the level of single neurons and astrocytes? If so, does the potentiation influence specific features of single neuronal responses and representations? In particular, is the potentiation a nonspecific increase in responses independent of sensory stimulus features, or does it selectively facilitate responses to stimuli that have been paired with NB stimulation?

The primary visual cortex (V1) provides an excellent model system to address these issues. Modulation by ACh in general and cholinergic drive from the NB in particular are known to influence V1 circuits in multiple ways, resulting in an enhancement of direction and orientation selectivity in V1 neurons (19–22), increase in attentional modulation of V1 neurons in behaving monkeys (23), and alteration in the reliability and synchrony of stimulus-evoked spikes in V1 neurons (24). Responses of mature V1 neurons to specific visual stimulus features have also been shown to be plastic and depend on the history of visual stimulation (25). Moreover, cortical astrocytes have previously been demonstrated to be an integral component of V1 circuits because they are visually responsive and are capable of modulating visually driven neuronal responses (26). We therefore examined the influence of NB-mediated cholinergic activation of astrocytes and neurons in mouse V1 in vivo, and the mechanisms of their interactions in V1 slices ex vivo, using both calcium imaging and electrophysiological recording. We show that pairing electrical stimulation of the NB with visual stimuli can induce potentiation of visual responses in V1 excitatory neurons. The potentiation is facilitated by astrocytes, which are activated by cholinergic inputs from the NB and, in turn, directly influence neuronal responses, and is abolished in mice that lack astrocyte calcium increases due to deletion of astrocytic inositol 1,4,5 trisphosphate receptor type 2 (IP_3R2). This astrocyte-mediated response potentiation is stimulus-specific, because pairing one stimulus orientation with NB stimulation selectively potentiates the visual response of the paired orientation over other unpaired orientations.

Results

Pairing NB and Visual Stimulation Potentiates Visual Responses in Excitatory Neurons in Vivo. We first investigated if paired NB and visual stimulation can induce potentiation of identified excitatory neuron responses. The NB was stimulated with an implanted bipolar electrode (*SI Materials and Methods*, *In Vivo Surgery*) (24), whereas responses of single visual cortical neurons in the supragranular layers were recorded with in vivo cell-attached recordings (Fig. 1 *A* and *D*, *Upper*). The stereotaxic accuracy of the implantation was determined by (*i*) localization of the electrode tip within the NB as assessed by acetylcholinesterase staining (24) (Fig. 1*B*) and (*ii*) the effect of stimulation on desynchronization of the interhemispheric electroencephalogram (24, 27) (Fig. 1*C*). Excitatory neurons were characterized by their "regular spiking" properties (28), including spike half-widths and peak-to-valley ratios (Fig. S1 *A* and *B*), and their responses before, during, and after the pairing paradigm were recorded at single-spike resolution for long durations. The visual stimuli consisted of gratings of

Author contributions: N.C., H.S., and M.S. designed research; N.C., H.S., J.S., G.P., and C.L. performed research; J.P. contributed new reagents/analytic tools; N.C., H.S., and G.P. analyzed data; and N.C. and M.S. wrote the paper.

The authors declare no conflict of interest.

This article is a PNAS Direct Submission.

[1]N.C. and H.S. contributed equally to this work.

[2]To whom correspondence should be addressed. E-mail: msur@mit.edu.

See Author Summary on page 16427 (volume 109, number 41).

This article contains supporting information online at www.pnas.org/lookup/suppl/doi:10.1073/pnas.1206557109/-/DCSupplemental.

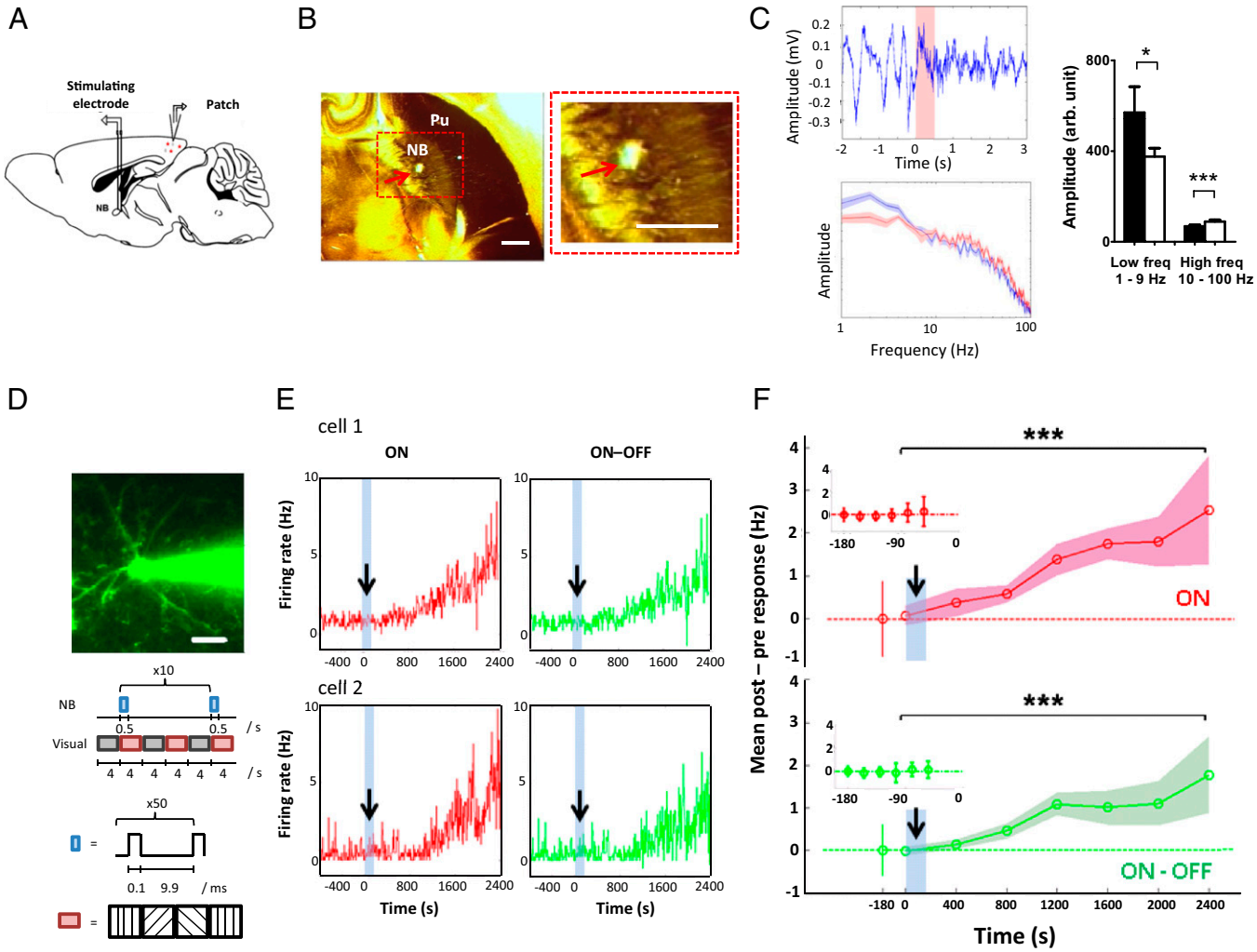

Fig. 1. Paired NB and visual stimulation potentiates visual responses in excitatory neurons in vivo. (*A*) Schematic illustration of cell-attached recordings from V1 neurons during paired NB and visual stimulation (50). (*B*) (*Left*) Localization of the stimulation electrode tract in the NB (red arrow), revealed by acetylcholinesterase histochemistry. Pu, putamen. (*Right*) Magnified view of the red box. (Scale bars, 500 μm.) (*C*) (*Upper Left*) Desynchronization of the interhemispheric EEG signal after NB stimulation at $t = 0$ s (pink bar). (*Lower Left*) Amplitude-frequency graph 1 s before (blue) and after (red) NB stimulation, averaged over 10 trials. (*Right*) NB stimulation induces a decrease in the amplitude of low-frequency events ($n = 9$ datasets; $^*P < 0.05$, paired t test) and an increase in high-frequency events ($n = 91$ datasets; $^{***}P < 0.0001$, paired t test), respectively. EEG desynchronization and/or acetylcholinesterase histochemistry was used to verify NB electrode placement in every experiment. (*D*) (*Upper*) Pyramidal neuron electroporated with green Alexa 488 dye by a glass pipette that forms a loose seal with it. (Scale bar, 20 μm.) (*Lower*) Schematic illustration of the paired NB and visual stimulation protocol. A visual stimulus (random orientation gratings, pink) was alternately presented with a blank gray screen (gray). NB trains (blue) were synchronized with the onset of each visual stimulus for 10 trials. (*E*) Examples of neurons that show potentiation of ON and ON–OFF responses with paired NB and visual protocol (blue shades with arrow). (*F*) Mean post-NB minus pre-NB response changes (firing rate, Hz) show potentiation of ON and ON–OFF visual responses in a population of neurons ($n = 6$ neurons in 6 animals; $^{***}P << 0.001$, paired t test comparing pre-NB with post-NB responses pooled across all 400-s time segments for both ON and ON–OFF responses). Blue-shaded bars with an arrow indicate the NB stimulation period. Color shades around means indicate SEM. (*Insets*) Stable baseline responses before NB stimulation. The x-axis labels indicate the start of the time segment analyzed.

random orientation designed to evoke robust responses and were presented alternately with blank gray screens (Fig. 1*D*, *Lower* and *SI Materials and Methods*, *Visual Stimulation*). Stimulating the NB with multiple trains of pulses, where each train (50 pulses at 100 Hz; *SI Materials and Methods*, *NB Stimulation*) was paired with a cycle of visual stimulus (Fig. 1*D*, *Lower*), induced a prominent sustained slow potentiation of visual responses in excitatory neurons lasting over 40 min (Fig. 1 *E* and *F*). The firing rates during the alternate visual stimulus and blank gray screen presentations were quantified as "ON" and "OFF" responses, respectively, whereas the ON responses relative to the preceding OFF responses were quantified as "ON–OFF." The increase was pronounced in both visual ON and ON–OFF responses (Fig. 1*F*: $n = 6$ neurons in 6 animals; $P << 0.001$). Thus, paired NB and visual stimulation reliably potentiates visually driven responses of regular spiking, presumably pyramidal V1 neurons.

In Vivo NB Stimulation Evokes Robust Calcium Responses in Visual Cortical Astrocytes via Muscarinic Receptors. Next, we use in vivo two-photon imaging (Fig. 2*A*, *Left*) to investigate if NB stimulation can activate V1 astrocytes. V1 astrocytes and neurons were loaded with the fluorescent calcium indicator Oregon Green 488 Bapta-1-AM (OGB1-AM), whereas astrocytes were loaded with the selective astrocytic marker sulforhodamine101 (SR101; Molecular Probes) (29) (Fig. 2*A*, *Right*). OGB1-AM fluorescence in astrocytes was monitored continuously with two-photon imaging during NB stimulation. First, we examined the

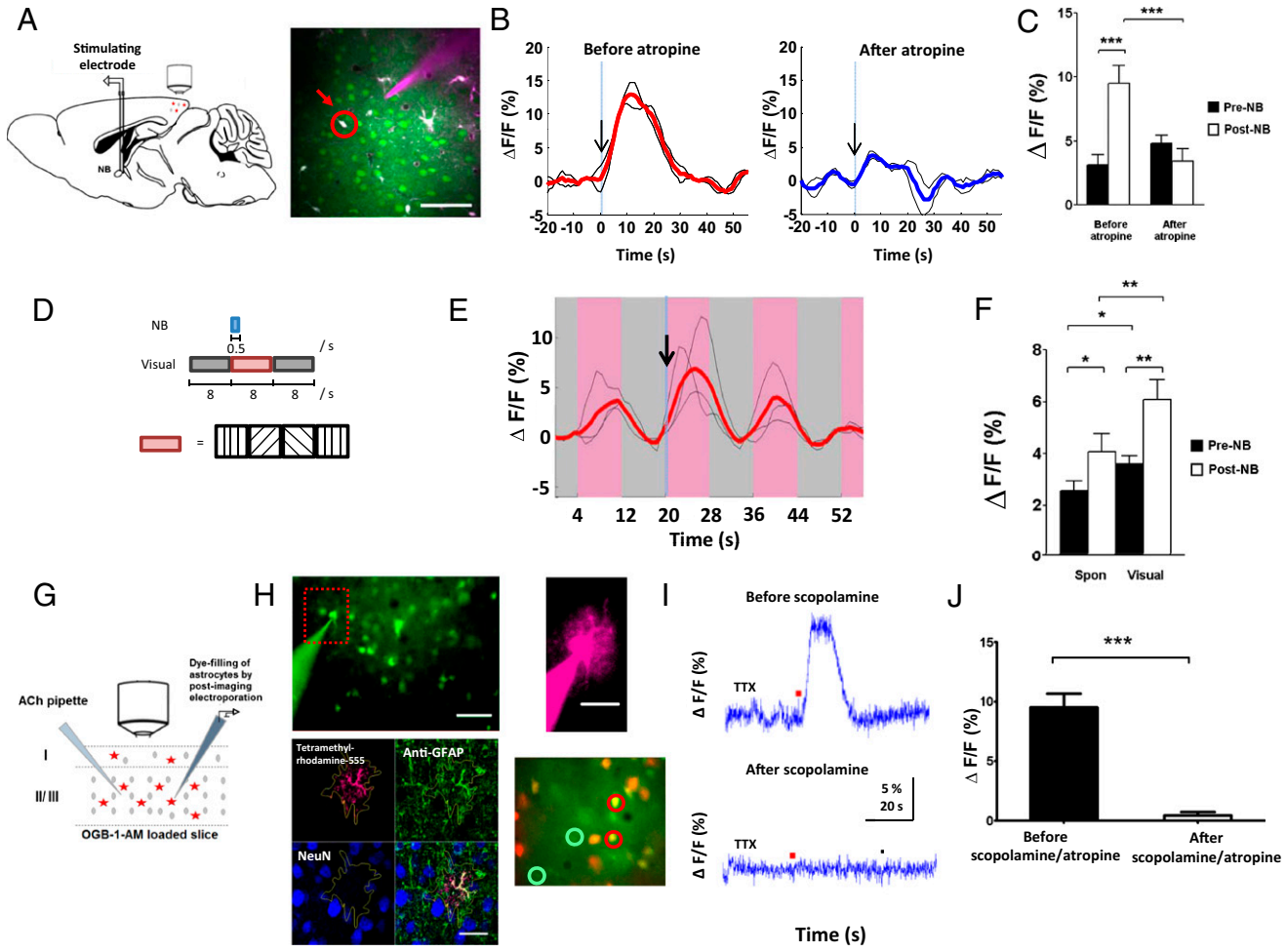

Fig. 2. In vivo NB stimulation and ex vivo ACh application directly induce robust calcium responses in visual cortical astrocytes via muscarinic receptors. (*A*) (*Left*) Schematic illustration of the experimental setup for two-photon calcium imaging during NB stimulation. (*Right*) Labeling of cortical astrocytes with OGB1-AM (green) and SR-101 (red) with a micropipette for pressure injection of atropine plus A594 to visualize drug spread. An astrocyte used in the analysis is circled in red. (Scale bar, 50 μm.) (*B*) Responses of astrocytes to brief NB stimulation (arrow) before and after the application of atropine. Black lines show examples of trial-averaged single-cell responses computed from three NB stimulation repeats; red and blue lines are means of the single-cell responses. (*C*) Population averages of NB stimulation-induced calcium responses in astrocytes before and after atropine application. Shown are responses of cells with trial-averaged post-NB responses greater than pre-NB responses (astrocytes: 17 of 26, $n = 3$ animals). $^{***}P < 0.001$. (*D*) Schematic illustration of the paired NB and visual stimulation protocol used. The random orientation grating stimulus (pink) was alternately presented with a blank gray screen (gray) across multiple cycles. A single brief train of NB pulses was synchronized with the onset of one visual stimulus cycle. (*E*) NB stimulation (arrow) facilitates visual responses in astrocytes. Pink/gray bars indicate time segments when a visual stimulus and a blank gray screen, respectively, were presented. Black and red lines are computed similarly as those in *B*. (*F*) Population average of NB stimulation-induced calcium responses in astrocytes before and after visual stimulation. Shown are 47 of 63 cells (5 animals) with significant visual responses ($^{*}P < 0.05$, paired *t* test comparing pre-NB responses before and after visual stimulation). $^{*}P < 0.05$; $^{**}P < 0.01$ by paired *t* test. (*G*) Schematic illustration of experimental setup for calcium imaging of OGB1-AM–loaded layer 2/3 astrocytes in V1 slices. ACh was pressure-ejected locally, and electroporated astrocytes were identified by immunohistochemistry (*SI Materials and Methods, Immunohistochemistry*). (*H*) (*Upper Left*) Fluorescence image of OGB1-AM–loaded astrocytes and neurons shows an electroporation pipette. (Scale bar, 50 μm.) (*Upper Right*) Tetramethylrhodamine-555 (T-555) dye-filled astrocyte. (Scale bar, 25 μm.) (*Lower Left*) That astrocyte is demarcated in yellow by extent of T-555, which colocalizes with anti-GFAP but not with neuronal nuclei (NeuN) immunohistochemistry. (Scale bar, 25 μm.) (*Lower Right*) Merged SR101 (red) and OGB1-AM (green) fluorescence images obtained during simultaneous calcium imaging of OGB1-AM–loaded astrocytes (circled red) and neurons (circled green), where the former is colabeled with SR101. (Scale bar, 50 μm.) (*I*) ACh (red dot; 50 mM, 0.2–1 s, 20 psi) induces TTX-insensitive calcium transients in astrocytes, which are abolished by the mAChR antagonist scopolamine (20 μM). (*J*) Population average of ACh-induced calcium responses in astrocytes before/after mAChR antagonists. Responses to scopolamine and atropine are similar and pooled (scopolamine, $n = 6$ astrocytes; atropine, $n = 2$ astrocytes; $^{***}P = 0.0001$, paired *t* test; $n = 4$ slices in 3 animals). Error bars indicate SEM. ΔF/F, time-lapse change in fluorescence normalized by the baseline fluorescence.

effect of a brief train of pulses applied to the NB (50 pulses at 100 Hz) on the spontaneous activity in astrocytes. Indeed, we observed robust increases in the calcium responses of astrocytes (Fig. 2*B*, *Left*: $n = 30$ of 44 astrocytes in 5 animals; $P < 0.0001$, paired *t* test, comparing population, trial-averaged responses before and after NB stimulation). When atropine, a muscarinic AChR (mAChR) antagonist, was delivered by a visualized pipette (Fig. 2*A*, *Right*), NB-evoked responses were reduced to pre-NB levels [Fig. 2 *B*, *Right*, and *C* ($n = 17$ NB stimulation-facilitated astrocytes in 3 animals; $P = 0.001$, paired *t* test, comparing responses before and after NB stimulation; $P < 0.001$, paired *t* test, comparing NB evoked responses before and after atropine application) and Fig. S2*A*]. Thus, responses of cortical astrocytes to NB stimulation are evoked by cholinergic modulation via mAChRs.

To examine how NB activation influences visual responses of astrocytes, we presented randomly oriented visual gratings synchronized to a single, brief train of pulses applied to the NB (Fig. 2*D*) while imaging astrocyte responses. Indeed, visual responses of

astrocytes were enhanced by NB stimulation [Fig. 2 *E* and *F* (n = 47 visually responsive astrocytes in 5 animals; $P < 0.01$, paired t test, comparing population average of visual responses pre- and post-NB) and Fig. S2*B*], showing that V1 cortical astrocytes are capable of integrating visual and cholinergic inputs.

ACh Stimulation in V1 Slices Evokes Calcium Responses in Astrocytes via Muscarinic Receptors. To examine the mechanisms underlying NB-evoked responses in astrocytes, we performed calcium imaging of astrocytes in slices of V1. Responses of OGB1-AM–loaded layer 2/3 astrocytes were imaged (Fig. 2*G*) before and after ACh application. Imaged astrocytes had small round somas with thin radiating processes revealed by OGB1-AM loading (Fig. 2*H*, *Upper Left*). The identity of the imaged astrocytes was further confirmed by colocalization of their dye-filled processes (Fig. 2*H*, *Upper Right*) with anti-GFAP immunohistochemistry (Fig. 2*H*, *Lower Left*) and with the astrocyte-selective marker SR101 (29) in selected experiments (Fig. 2*H*, *Lower Right*). To mimic brief NB stimulation, we applied a brief pulse (0.2–1 s) of ACh, which evoked robust calcium transients in astrocytes (Fig. 2*I*, *Upper*). These responses were TTX-insensitive (Fig. 2*I*) and were abolished by the mAChR antagonists scopolamine and atropine (Fig. 2 *I*, *Lower*, and *J*: $n = 8$ astrocytes in 3 animals; $P = 0.0001$, paired t test). Immunohistochemistry confirmed that mAChRs were expressed on GFAP-expressing astrocytes (Fig. S3 *A* and *B*). To mimic prolonged NB stimulation, we bath-applied ACh, which caused an increase in the frequency and duration of calcium transients lasting for several minutes (Fig. S3 *C–F*). These findings, together with in vivo results (Fig. 2 *A–F*), indicate that V1 astrocytes are direct targets of NB stimulation-evoked cholinergic modulation via mAChRs (10, 11) and that the time scale of their calcium responses depend on the mode of ACh application and not on neuronal action potentials.

Cholinergic Activation of Astrocytes Contributes to Prolonged Depolarizing Responses in Excitatory Neurons via Calcium-Mediated Processes. The NB- and ACh-induced astrocyte responses suggested that the sustained slow potentiation of excitatory neuronal responses following paired NB and visual stimulation (Fig. 1 *D–F*) could be a contribution by astrocytes to neuronal plasticity, based on previous evidence that hippocampal astrocytes play a role in synaptic plasticity (13–15) and facilitate neuronal responses via gliotransmitter release (30, 31) or regulation of glutamate uptake (32).

We first tested the hypothesis that cholinergic activation of astrocytes can contribute to cholinergic facilitation of neuronal responses by performing whole-cell patch recordings in V1 slices (Fig. 3*A*). Excitatory neurons, identified by their electrophysiological regular spiking and morphological characteristics, responded to a brief pulse of ACh with slow, prolonged depolarization (Fig. 3 *E–G*, *Upper*: $n = 50$ of 50 neurons), which was TTX-insensitive (Fig. S4: $n = 10$; $P > 0.9$, paired t test). We examined the mechanisms behind the ACh-induced slow depolarization further by blocking calcium responses in astrocytes (Fig. 3*A*). Astrocytic calcium was chelated through patch-loading electrophysiologically characterized astrocytes (Fig. 3*B*) with the cell-impermeable calcium chelator 1,2-Bis(2-aminophenoxy)ethane-*N*,*N*,*N*′,*N*′-tetraacetic acid (BAPTA) and allowing BAPTA to travel within the local syncytium of astrocytes via gap junctions (33, 34). The spread of BAPTA was assessed by Alexa Fluor 594 (A594; Molecular Probes) dye included in the patch pipette and determined to be ~150 μm from the patched astrocyte within 30–45 min of dialysis (Fig. 3*C*). BAPTA effectively blocked ACh-induced calcium transients in the dialyzed astrocytes (Fig. 3*D*). Excitatory neurons within 100 μm of the patched astrocytes (Fig. 3*C*) were recorded after BAPTA dialysis. The amplitude of the ACh-induced slow depolarization in neurons within the dialyzed astrocytic network was reduced compared with that in control conditions (Fig. 3*E*), either without astrocyte patch ($n = 9$ neurons; $P < 0.001$, t test) or in the presence of astrocytes dialyzed with A594 without BAPTA ($n = 9$ neurons; $P < 0.0001$, t test) (Fig. 3*H*). The slow neuronal depolarizations were mediated by mAChRs as they were abolished by atropine (Fig. 3 *F* and *I*: atropine, $n = 18$ neurons in 13 animals; $P < 0.001$, paired t test), consistent with our previous demonstration that ACh-induced astrocyte calcium transients were mAChR-mediated (Fig. 2 *B*, *C*, and *I–J*). These data therefore demonstrate that cholinergic activation of astrocytes can contribute to cholinergic facilitation of mAChR-mediated neuronal responses via increase of intracellular calcium.

Cholinergic Activation of Astrocytes Evokes Slow NMDA Receptor-Mediated Currents in Neurons. Earlier work has demonstrated that gliotransmitters released by astrocytes can act on the NR1/NR2B subunits of extrasynaptic NMDA receptors (NMDARs) in neurons (35, 36). These subunits have slow kinetics (37–39) and have been proposed to give rise to slow currents observed in neurons when adjacent astrocytes are activated (12, 36, 40). To investigate if NMDA-mediated currents underlie the astrocyte-evoked cholinergic responses in neurons, we performed whole-cell voltage-clamp recordings in which slow currents were defined and discriminated from miniature excitatory postsynaptic currents by their differential time courses (Fig. 4 *A–C*, Fig. S5 *A* and *B*, and *SI Materials and Methods*, *Analysis of Slow Currents*). Indeed, ACh induced an increase in the frequency of TTX-insensitive slow currents (Fig. 4 *D–F*, *Upper*, and *G*; Table S1 and Fig. S5*C*: $n = 18$ neurons in 9 animals; $P < 0.0001$, paired t test). These ACh-induced slow currents were atropine-sensitive (Fig. 4 *E* and *G* and Table S1: $n = 10$ neurons in 5 animals; $P < 0.02$, paired t test comparing ACh-induced slow current frequency before and after atropine application). To investigate if these currents have an astrocytic origin, double-patch experiments were performed in which a pyramidal neuron was patched and a neighboring astrocyte was contacted with a BAPTA-containing patch pipette in a cell-attached configuration, keeping the membrane intact to prevent BAPTA diffusion into the astrocyte. ACh-induced slow currents in the pyramidal neurons were first recorded before the seal between the astrocyte and BAPTA-containing patch pipette was broken to allow BAPTA dialysis of the astrocyte syncytium. After 30–45 min of BAPTA dialysis, a reduction of ACh-induced slow currents was observed (Fig. 4 *D*, *Lower*, and *G* and Table S1: $n = 5$ neurons in 4 animals; $P < 0.006$, paired t test comparing ACh-induced slow current frequency before and after BAPTA dialysis of astrocytes). In a similar set of experiments in which excitatory neurons were patched after astrocytic BAPTA dialysis, we also observed a reduction in the frequency of ACh-induced slow currents [Fig. S5*C*: $P << 0.001$, t test comparing ACh-induced slow current frequency without ($n = 18$ neurons) and with ($n = 11$ neurons) BAPTA dialysis of astrocytes]. The reduction of slow currents was further confirmed not to be due to the extracellular action of BAPTA (Fig. S5*D*). Both the ACh-induced slow currents and slow depolarizations in neurons were reduced in the presence of D-2-Amino-5-phosphonovaleric acid (D-APV), indicating that they are mediated by NMDARs (Slow currents in Fig. 4 *F* and *G* and Table S1: $n = 10$ in 7 animals; $P = 0.0001$, paired t test comparing ACh-induced slow current frequency before and after D-APV application; slow depolarization in Fig. 3 *G* and *I*: $n = 8$ neurons in 8 animals; $P < 0.003$, paired t test). Although we cannot determine the causal relationship between the ACh-induced slow currents and slow depolarization, their similar insensitivity to TTX (Fig. 4 *D–F* and Fig. S4) and similar sensitivity to BAPTA dialysis, D-APV, and atropine (Figs. 3 *E–I* and 4 *D–G*), as well as comparable durations (mean duration of slow depolarization = 76.6 ± 10.25 s, $n = 24$; duration of increase in slow current frequency = 60–120 s, $n = 13$; Fig. 4 *D–F*, *Upper*) and long peak and valley latency (Figs. 3*E* and 4 *A*, *B*, and *D*), suggest a correlation between the two phenomena. Considering the low slow-current frequency, it is possible that the depolarization of the cellular membrane induced by these slow currents favors the

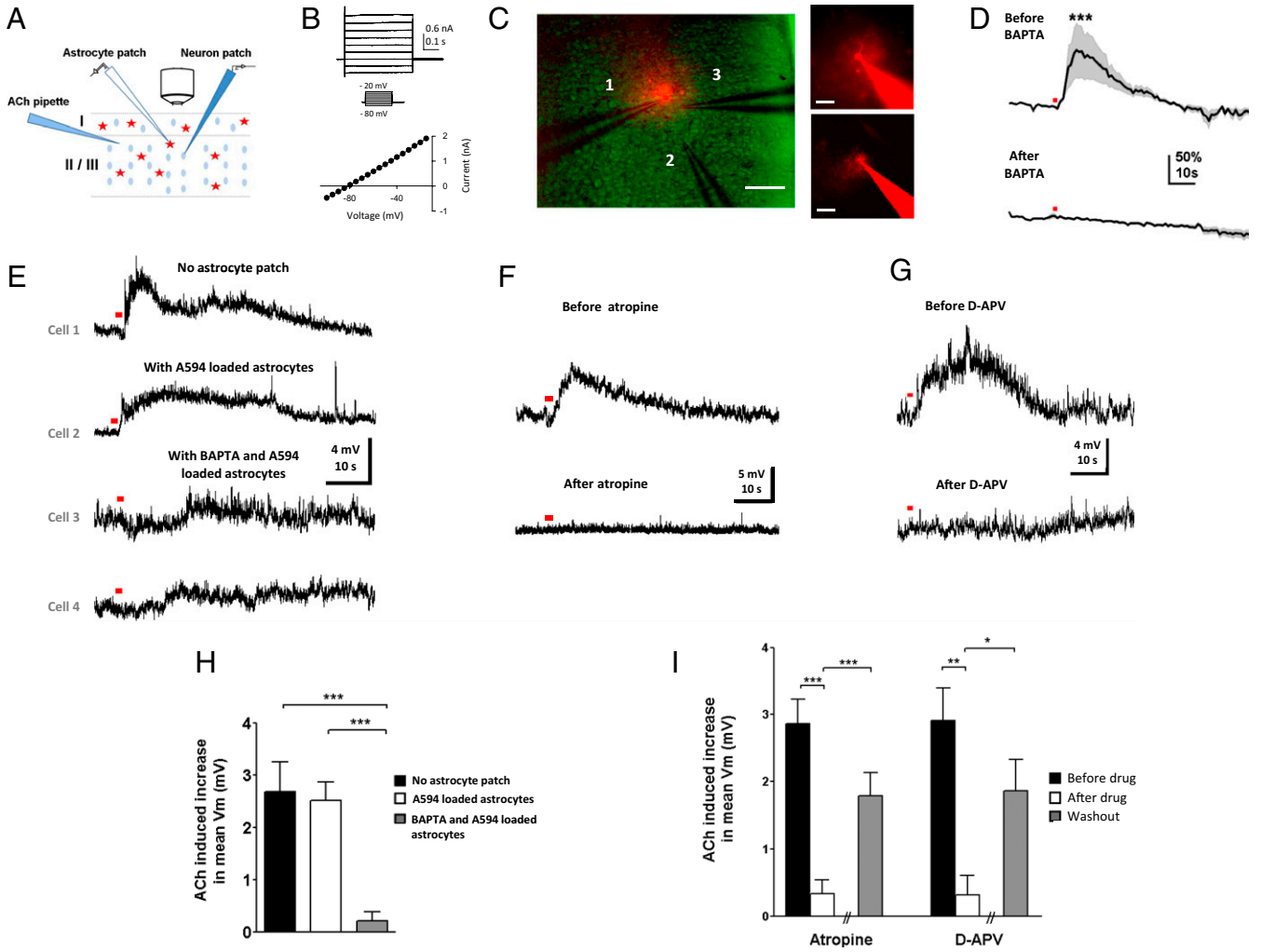

Fig. 3. Cholinergic activation of astrocytes contributes to prolonged depolarizing responses in excitatory neurons ex vivo. (*A*) Schematic illustration of slice experimental setup. Calcium responses of layer 2/3 V1 astrocytes were imaged after ACh application (10 mM, 200 ms, 20 psi, unless indicated otherwise), before/after being loaded with A594 and/or calcium chelator BAPTA by whole-cell patch-clamp. Neurons were patched immediately after A594 and/or BAPTA dialysis within astrocyte syncytium. (*B*) Electrophysiological characteristics of an astrocyte, with the I-V curve showing negative resting basal membrane potential (V_m) and absence of active membrane currents. (*C*) (*Left*) Relative positions of an astrocyte patch pipette (1), ACh pipette (2), and neuronal patch pipette (3) as indicated. (Scale bar, 100 μm.) The range of spacing between ACh and patch pipettes in all experiments was 20–100 μm. (*Right*) Spread of A594 (and BAPTA) in the syncytium (*Lower*) within 30–45 min of patching an astrocyte identified by its small round soma with thin radiating processes (*Upper*). (Scale bars: *Lower*, 100 μm; *Upper*, 25 μm.) (*D*) Population-averaged calcium responses in astrocytes to ACh application (red dot, 1 s, 20 psi) (n = 35 astrocytes in 4 animals) before and after BAPTA loading (50 mM). ***P << 0.001, paired t test comparing population-averaged responses during 10-s post-ACh application before and after BAPTA loading. SEM is represented by shading about the mean. (*E*) Compared with control responses from patch-clamped excitatory neurons recorded without an astrocyte patch (cell 1) and with A594 loading of the astrocyte syncytium (cell 2), the amplitude of ACh-induced slow depolarization is reduced in excitatory neurons after BAPTA/A594 dialysis of adjacent astrocytes (cells 3 and 4). (*F* and *G*) Bath application of atropine (10–100 μM) and D-APV (50 μM) drastically reduced the slow depolarization amplitude. (*H*) Population average of ACh-induced increase in mean V_m of (*i*) neurons patched without loading astrocytes (n = 9, randomly sampled without replacement from a large pool of 50 neurons), (*ii*) neurons patched after loading astrocytes with A594 (n = 9 neurons and n = 4 astrocytes in 4 animals), and (*iii*) neurons patched after loading astrocytes with BAPTA and A594 (n = 9 neurons and n = 8 astrocytes in 6 animals). $P > 0.8$; $P < 0.001$; $P < 0.0001$ by t test comparing (*i*) and (*ii*), (*i*) and (*iii*), and (*ii*) and (*iii*), respectively. (*I*) Population average of ACh-induced increase in mean V_m of neurons before/after bath application and washout of atropine (n = 18 and n = 8 of 18 with washout in 13 animals) and D-APV (n = 8 and n = 4 of 8 with washout in 8 animals). The ACh-induced increase in mean V_m was calculated as the difference between mean V_m during 15-s pre-ACh and post-ACh application. *$P < 0.05$; **$P < 0.01$; ***$P < 0.001$ by paired t test comparing before/after drug and t test comparing after drug/washout. Error bars indicate SEM.

development of ACh-induced prolonged depolarization. Collectively, these findings indicate that cholinergic excitation of astrocytes via mAChRs leads to calcium-mediated processes that, in turn, evoke NMDAR-mediated facilitatory responses, including the neuronal slow currents and slow depolarization.

Astrocytic IP_3R2-Mediated Calcium Mediates NB Stimulation-Evoked Potentiation of Visual Responses in Excitatory Neurons. We next investigated if cholinergic activation of astrocytes can contribute to the NB-mediated potentiation of visual responses in excitatory neurons observed in vivo (Fig. 1 *E* and *F*). For this purpose, we used conditional IP_3R2 KO mice (IP_3R2-cKO) (Fig. S6 and *SI Materials and Methods*, *Mice*), where the astrocytic IP_3R2, previously shown to be the only IP_3R (41) that mediates agonist-induced calcium responses in astrocytes (33, 42), is specifically knocked out in GFAP-expressing astrocytes (Fig. 5*A*). In WT mice 77 of 80 GFAP-expressing cortical astrocytes (96.3%) colocalized with IP_3R2; in IP_3R2-cKO mice the fraction was 7 of 90 (7.8%). [Because the evidence for IP_3R2 expression in neurons remains inconclusive (41, 42), the IP_3R2-cKO mice were used instead of the

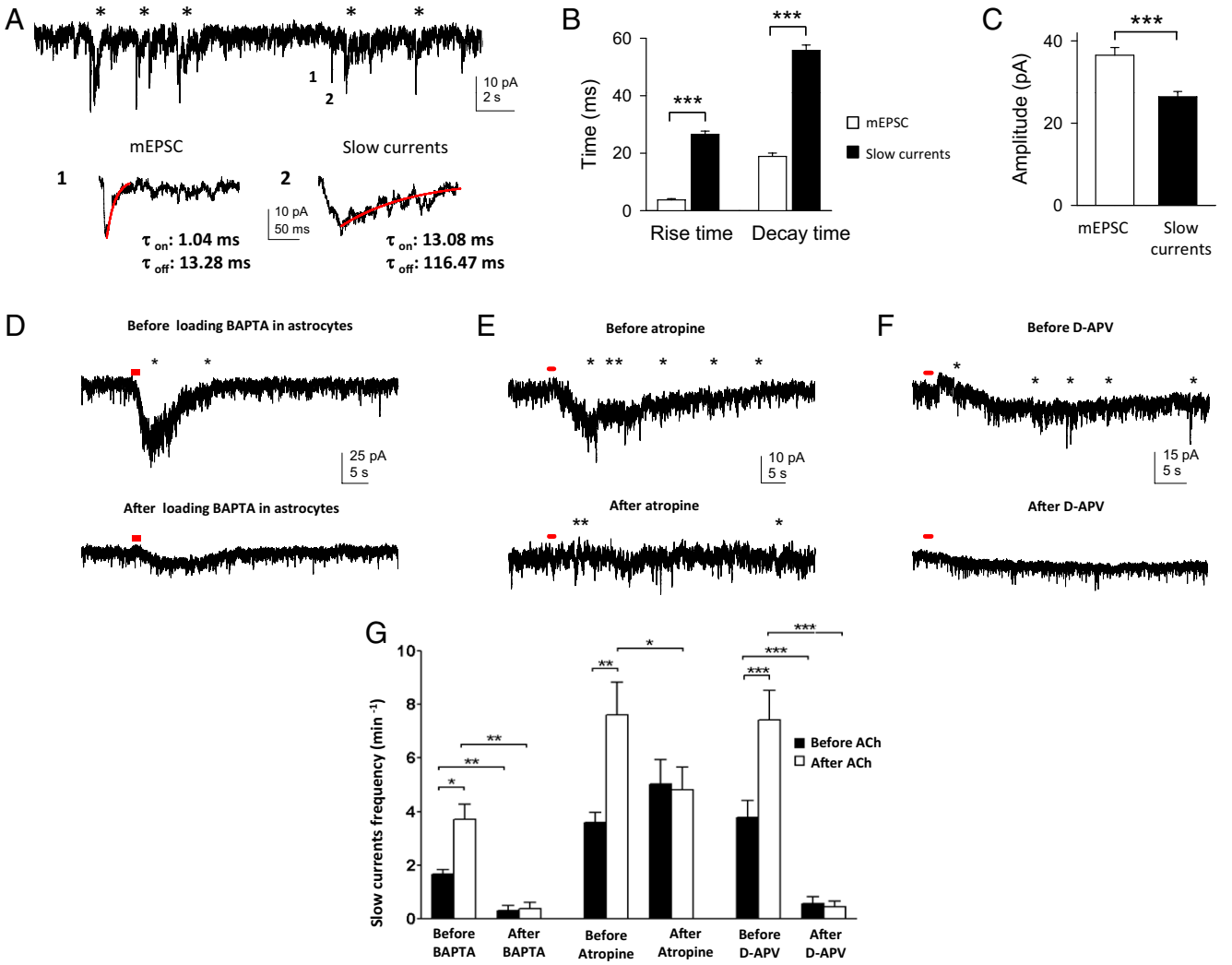

Fig. 4. Cholinergic activation of astrocytes contributes to an increase in TTX-insensitive slow currents in excitatory neurons via calcium-mediated processes that act on neuronal NMDARs. (*A*) Whole-cell neuronal recording in which slow currents (labeled with asterisks) were discriminated from miniature excitatory postsynaptic currents (mEPSCs) based on their time course. (*Lower*) Expanded trace shows the amplitude and time course of (1) a mEPSC and (2) a slow-current event. τ_{on} and τ_{off}, time constants of activation and deactivation (delineated by the red traces). (*B*) Comparison of the mean rise and decay times between mEPSCs and slow currents (rise and decay times: ***$P << 0.001$, *t* test). (*C*) Comparison of the mean amplitudes between mEPSCs and slow currents (***$P << 0.001$, *t* test). *B* and *C* were computed from 75 events in 15 neurons. Error bars indicate SEM. (*D–F*) ACh (red dot, 10 mM, 200 ms, 20 psi) induces an increase in the frequency of TTX-insensitive slow currents (labeled with asterisks) in a neuron (*Upper*), which is reduced after (*D*, *Lower*) BAPTA dialysis of astrocytes, (*E*, *Lower*) bath application of atropine (50 μM), and (*F*, *Lower*) bath application of D-APV (50 μM). In *D*, unlike in Fig. 3, neurons were patched first and their cholinergic responses were assessed before and after BAPTA dialysis of astrocytes. (*G*) Population average of TTX-insensitive slow currents before and after ACh application in the following conditions: before/after BAPTA dialysis, before/after atropine, and before/after D-APV. *$P < 0.05$; **$P < 0.01$; *** $P <$ 0.001 by paired *t* test. Error bars indicate SEM.

full IP_3R2 KO mice]. We first performed calcium imaging (Fig. 2*G*) in V1 slices of adult IP_3R2-cKO and WT (control) animals. Although ACh induced calcium responses in astrocytes of WT mice, no astrocytic calcium responses were observed in the IP_3R2-cKO mice (Fig. 5*B*). We next performed whole-cell patch recordings in V1 slices of adult IP_3R2-cKO and WT animals. The amplitude of the ACh-induced slow depolarization in IP_3R2-cKO regular spiking neurons was indeed drastically reduced compared with that in WT (Fig. 5*C*: $n = 5$ WT and $n = 5$ IP_3R2-cKO neurons in 2 animals each; $P < 0.001$, *t* test). When the NB was stimulated with multiple trains of pulses, where each train was paired with visual stimulation in the IP_3R2-cKO animals in vivo using the same protocol/analysis as in WT animals (Fig. 1*D*), no sustained potentiation was observed (Fig. 5*D*: $n = 5$ neurons in 4 animals; $P >$ 0.1, paired *t* test comparing pre-NB responses with post-NB responses pooled across all 400-s time segments for ON, ON–OFF, and OFF responses). The neurons in the IP_3R2-cKO animals had similar electrophysiological properties as those in the WT animals (Fig. S7); therefore, the lack of sustained potentiation in the IP_3R2-cKO animals cannot be attributed to unintended secondary effects due to abnormal electrophysiology in the transgenic mice. These data therefore confirm that astrocytic IP_3R2-mediated calcium plays a significant role in the potentiation of visual responses in excitatory neurons following prolonged pairing of NB stimulation with visual stimulation.

NB-Induced Cholinergic Activation of Astrocytes Contributes to Potentiation of Stimulus-Specific Responses. The NB stimulation-evoked, astrocyte-mediated potentiation of visual responses could be a general increase in neuronal responsiveness, such that responses to any visual stimulus are indiscriminately enhanced, or it could reflect a specific facilitation of particular visual stimuli.

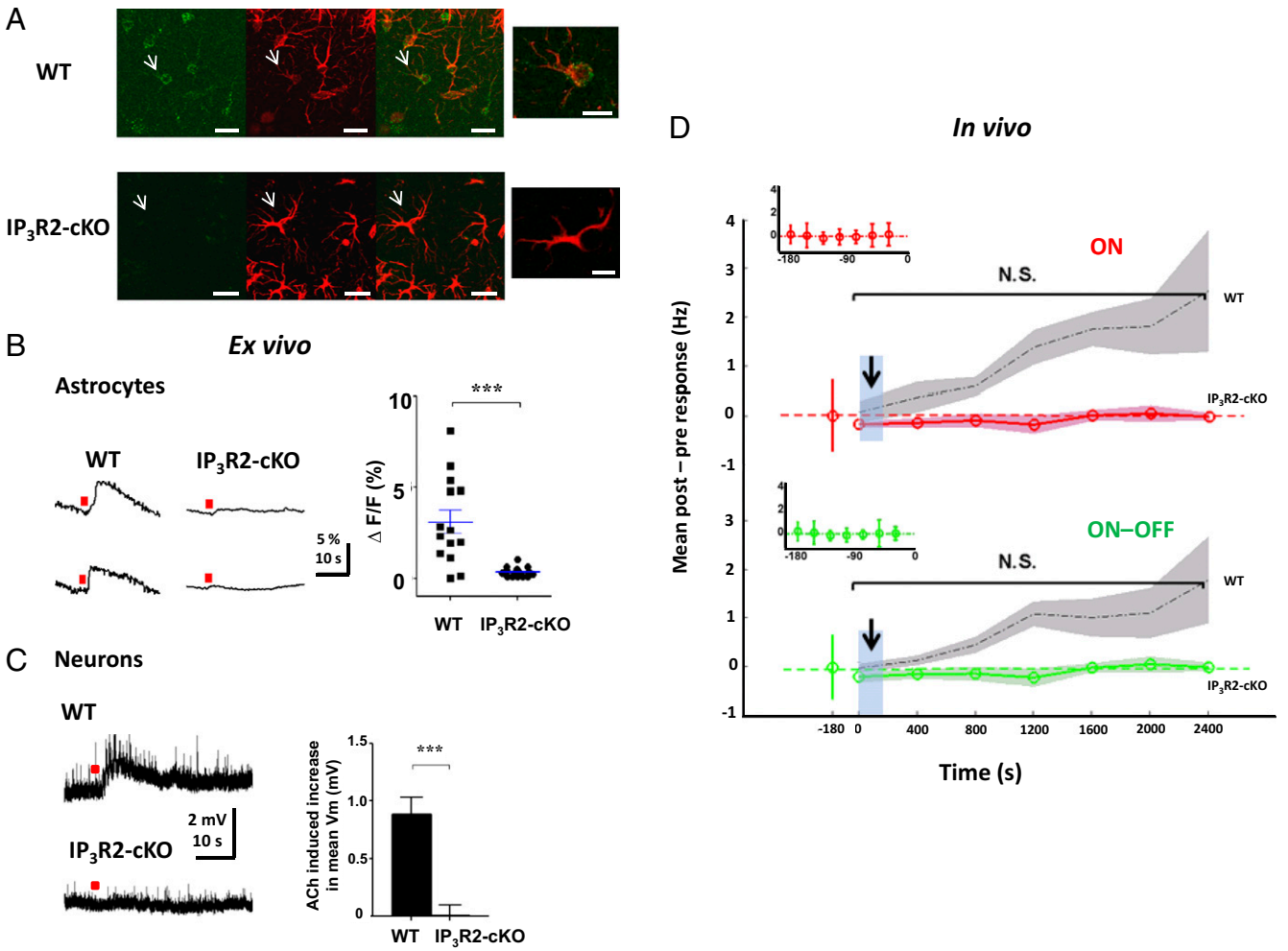

Fig. 5. Deletion of astrocyte IP_3R2 receptors abolishes ACh-induced depolarizing responses in excitatory neurons ex vivo and NB-induced potentiation of visual responses in vivo. (*A*) Immunohistochemical staining of layer 2/3 cortical astrocytes in WT animals (*Upper*) and IP_3R2-cKO animals (*Lower*) (2 animals each), with anti-IP_3R2 (*Left*) and anti-GFAP (*Center*), and showing colocalization of IP_3R2 on astrocytes in WT but not in IP_3R2-cKO animals due to highly reduced IP_3R2 staining in the latter (*Right*). (Scale bar, 20 μm.) (*Far Right*) Image shows a magnified image of the astrocyte marked by arrow in the previous images. (Scale bar: 10 μm.) (*B*) (*Left*) Local ACh application (red dot) evokes calcium responses in astrocytes in WT but not in IP_3R2-cKO adult slices. (*Right*) Magnitude of astrocyte calcium responses in WT (n = 14 astrocytes in 2 animals) and IP_3R2-cKO (n = 24 astrocytes in 2 animals). ***$P < 0.0001$, t test. (*C*) (*Left*) Local ACh application (red dot) evokes prolonged depolarizing responses in neurons in WT but not in IP_3R2-cKO adult slices. (*Right*) Population average of ACh-induced increase in mean basal membrane potential (V_m) of neurons in WT (n = 5 neurons in 2 animals) and IP_3R2-cKO (n = 5 neurons in 2 animals). ***$P < 0.001$, t test. (*D*) Mean post-NB minus pre-NB response changes (firing rate, Hz) in IP_3R2-cKO animals (red and green traces), following multiple pairings of NB stimulation trains with visual stimuli (identical to Fig. 1*D*), show absence of facilitation of visual responses (n = 5 neurons in 4 adult animals; $P > 0.1$, paired t test comparing pre-NB responses with post-NB responses pooled across all 400-s time segments for both ON and ON–OFF responses). Black dotted traces with gray shades are WT responses from Fig. 1*F*. Blue-shaded bars with an arrow indicate the NB stimulation period. Color shades around means indicate SEM. (*Insets*) Stable baseline responses before NB stimulation. N.S., nonsignificant.

To discriminate between these possibilities, we performed single-unit recordings from neuronal populations (Fig. 6*A*) in both WT and IP_3R2-cKO mice while simultaneously stimulating NB electrically and presenting gratings of a specific orientation as extrinsic visual stimulation. Responses to nine orientations each 20° apart, including an arbitrarily chosen orientation for the paired NB and visual orientation stimulation (conditioned orientation), were measured before and after the pairing protocol. Blank gray screens were interleaved between each orientation presentation. We observed an increase in the firing rates (Fig. 6*B*) as well as in normalized postresponses minus preresponses at the conditioned orientation in WT animals (ON–OFF responses are shown in Fig. 6 *C*, *Left,* and *D*, *Upper*: $n = 41$ neurons; $P < 0.001$, Wilcoxon rank-sum test comparing responses before and after pairing protocol; ON responses are shown in Fig. S8 *A* and *C*, *Upper*: $P < 0.001$, Wilcoxon rank-sum test comparing responses before and after pairing protocol). Interestingly, this increase was specific to the conditioned orientation because the facilitation at the conditioned orientation was significantly greater than at unconditioned orientations, with the latter showing no change in response (Fig. 6 *B*, *C*, *Left*, and *D* and Fig. S8 *A* and *C*). Recovery of this facilitation was observed earlier (Fig. S8*D*) than when NB stimulation was paired with random orientations (Fig. 1*F*), possibly due to reversal of synaptic modifications (43) induced by exposure to orientations other than the conditioned orientation after the pairing protocol (during assays of the postconditioning effects). In sum, these findings demonstrate that pairing NB stimulation with a specific visual orientation induces a highly specific potentiation of the conditioned orientation over unconditioned orientations in WT animals.

In the IP_3R2-cKO animals, no potentiation at the conditioned orientation was observed after the pairing protocol. Instead, a slight response depression was surprisingly revealed (Fig. 6 *B*,

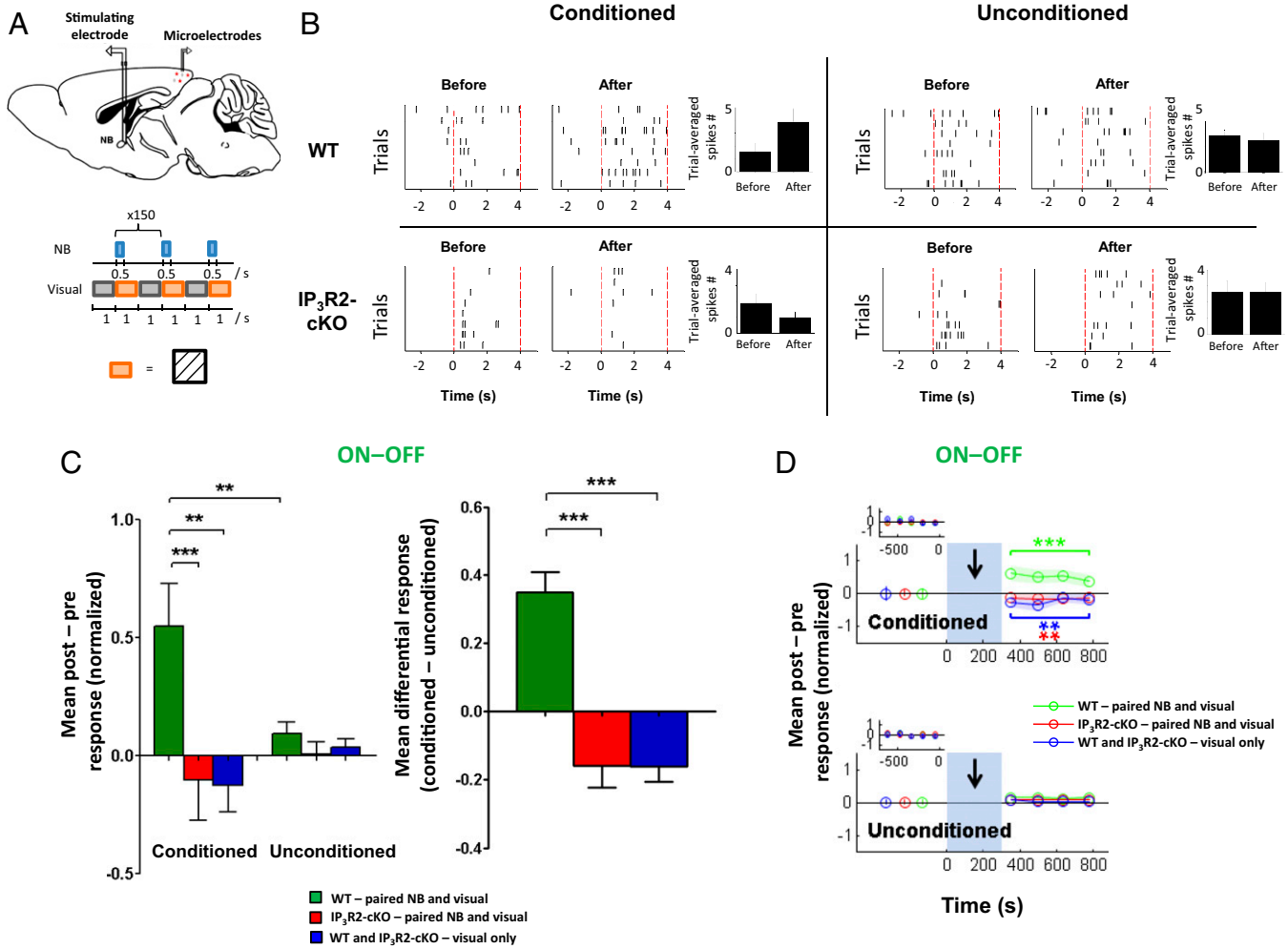

Fig. 6. Cholinergic activation of astrocytes contributes to stimulus-specific potentiation. (*A*) Schematic illustration of single-unit recordings from V1 neurons *(Upper)* and the protocol used during paired NB and visual stimulation (*Lower*). A visual grating of arbitrary orientation (orange) was alternately presented with a blank gray screen (gray); NB stimulation was synchronized with the onset of the visual stimulus for 150 trials. (*B*) Raster plots show examples of neuronal responses from a WT animal and an IP_3R2-cKO animal to a conditioned orientation (*Left*) and an unconditioned orientation (*Right*) before and after the pairing protocol. Presentation of the conditioned orientation is indicated by dotted red lines (0–4 s). Trial-averaged number of spikes for the example neurons (*Left*) is shown in bar graphs (*Right*). (*C*) (*Left*) Population mean of normalized post-NB minus pre-NB responses (ON–OFF) at conditioned and unconditioned orientations in WT and IP_3R2-cKO animals under different protocols. Control (visual-only) responses in WT and IP_3R2-cKO animals were similar (Fig. S8*E*) and are pooled for clarity (*SI Materials and Methods, Single-Unit Recording* and Table S2, statistical comparisons). $^{**}P < 0.01$, Wilcoxon rank-sum text. (*Right*) Mean differential responses (conditioned – unconditioned orientations). $^{***}P < 0.0001$, Wilcoxon rank-sum test. Error bars indicate SEM. WT (n = 5 animals): paired, n = 41 neurons; visual-only, n = 24 neurons. IP_3R2-cKO (n = 4 animals): paired, n = 45 neurons; visual-only, n = 21 neurons. (*D*) Time course of mean normalized post-NB minus pre-NB responses (ON–OFF) at conditioned (*Upper*) and unconditioned (*Lower*) orientations. Blue-shaded bars with an arrow indicate the NB stimulation period. (*Insets*) Pre-NB baseline responses were averaged over four trials and are shown. Postpairing responses at the conditioned orientation were significantly enhanced in WT animals (green). Responses were suppressed in the visual-only condition (blue; $P < 0.01$) and in IP_3R2-cKO animals after pairing (red; $P < 0.01$). $^{**}P < 0.01$; $^{***}P < 0.001$ by Wilcoxon rank-sum test comparing responses before and after NB pairing.

C, *Left*, and *D*, *Upper* and Fig. S8 *A* and *C*, *Upper*). The population mean conditioned response minus the unconditioned response in the IP_3R2-cKO mice showed a reversal in signs of conditioned responses, in marked contrast to the findings in the WT experiments (Fig. 6*C*, *Right* and Fig. S8*B*: $P < 0.0001$ comparing mean differential ON–OFF and ON responses in WT and IP_3R2-cKO paired experiments: n = 41 WT neurons and 45 IP_3R2-cKO neurons).

In additional control experiments in which the same visual stimuli were presented without NB stimulation (visual-only experiments), a similar reversal in signs of conditioned responses was observed (Fig. 6 *C* and *D* and Fig. S8 *A*–*C*: $P < 0.0001$ comparing mean differential responses, both ON–OFF and ON, between WT paired and visual-only experiments). Visual-only responses in WT and IP_3R2-cKO animals were similar (Fig. S8*E*). Conditioned responses were depressed to similar extents in the visual-only experiments, as well as in the IP_3R2 KO paired experiments (Fig. 6*C*, *Right* and Fig. S8 *B* and *E*: $P > 0.05$ for each comparison). Collectively, these findings show that the potentiation observed at the conditioned orientation requires both NB activation and intact astrocytic IP_3R2-mediated calcium elevation. The absence of either of these two factors changes the sign of conditioned responses, indicating that, by itself, the prolonged orientation-specific visual stimulation in the training protocol induces cortical response suppression, likely via adaptation mechanisms that have previously been shown to be reliably evoked by similar prolonged orientation-specific stimulation (25). (This phenomenon is absent in the IP_3R2-cKO responses measured in Fig. 5*D*, likely because the random orientation gratings used for pairing constitute a rapid presentation of drifting gratings of multiple orientations, and thus do not induce orientation-

specific adaptation.) The presence of NB stimulation paired with single-orientation stimulation, however, decisively counters this adaptation-induced suppression in WT animals but not in IP_3R2-KO animals. In sum, these data show that astrocyte calcium can mediate an NB-evoked stimulus-specific potentiation of V1 neuron responses that overrides adaptation-induced response suppression in these neurons.

Discussion

We have demonstrated that repeated NB stimulation paired with visual stimulation in vivo leads to prolonged potentiation of visual responses in V1 excitatory neurons. Previous work in rat auditory cortex has shown that NB stimulation paired with an auditory stimulus leads to significant cortical plasticity exemplified by changes in receptive fields (2, 6) and reorganization of cortical maps (3–5). Our work extends these findings by revealing the critical role of astrocytes in mediating this NB-induced cortical plasticity through their direct activation by cholinergic modulation via muscarinic receptors. Although we cannot rule out a direct facilitatory effect of NB stimulation on pyramidal neurons, the predominant contribution to the potentiation in neurons seems to be from an astrocytic calcium-driven mechanism, because removal of IP_3R2-mediated astrocytic calcium blocks NB-induced potentiation in vivo, whereas chelation of intracellular astrocytic calcium abolishes ACh-induced neuronal depolarization and slow currents ex vivo.

Recent reports using combined somatosensory and cholinergic stimulation have shown that cholinergic-activated astrocytes can induce synaptic plasticity (17, 18). However, it remained unknown if this plasticity reflects a general increase of cortical responsiveness or a more specific potentiation at the stimulus and circuit level. Using visual cortex as a model system, together with cell-attached and single-unit recordings, we were able to apply a more refined stimulus protocol and address the question at a single-cell level. We find that the astrocyte-mediated potentiation is indeed stimulus-specific, because pairing a grating of a particular orientation with NB stimulation induces a highly specific increase in response to the paired orientation but not to unpaired orientations. Because individual synapses on superficial layer V1 neurons convey specific orientation information (44), the influence of astrocyte-mediated plasticity has to be highly precise and even synapse-specific, and this suggests an intimate organization of astrocytes or their domains with respect to the synapses that convey and generate orientation-specific responses. Indeed, such organization is suggested by matched response features of neurons and adjacent astrocytes in V1 (26).

The generation and plasticity of orientation-selective responses in V1 requires both feed-forward inputs from the thalamus and recurrent inputs within the cortex (45, 46) and can be powerfully altered by top-down influences (47). NB inputs have also been implicated in top-down processes, including attention (23). Our findings indicate that astrocyte-mediated mechanisms, potentially through astrocytic calcium-dependent release of gliotransmitters that act on neuronal NMDARs, can induce a plasticity cascade in synapses and alter orientation-specific responses. Candidate ligands include glutamate (36) and D-serine [(15), compare with (48)]. Alternatively, the potentiation can be mediated by astrocytic calcium-dependent regulation of extracellular glutamate (26) or extracellular potassium (49), which may indirectly lead to NMDAR-mediated responses. Further investigation, however, is required to understand them in the context of NB-mediated potentiation. Regardless of the mechanism, our findings reveal an important role of astrocytes in NB-induced cortical plasticity and highlight their role as partners with neurons in restructuring specific circuits that govern stimulus-specific cortical responses.

Materials and Methods

C57BL/6 mice and IP_3R2-cKO mice older than 2 wk of age and older than 6 wk of age were used for ex vivo and in vivo experiments, respectively. All experiments were performed under protocols approved by the Animal Care and Use Committee, Massachusetts Institute of Technology, and conformed to National Institutes of Health guidelines. For in vivo two-photon calcium imaging, as well as cell-attached and single-unit experiments, mice were anesthetized with urethane or a fentanyl/midazolam/medetomidine mixture before craniotomy and NB electrode and EEG probe implantation. The NB was stimulated with either a single train or multiple trains of pulses, paired with presentation of either random or single-orientation visual gratings. EEG recordings during the experiment and acetylcholinesterase histochemistry after the experiment were performed to verify the stereotaxic accuracy of NB stimulation. Ex vivo slice experiments were performed for calcium imaging and whole-cell recording. Anti-GFAP, neuronal nuclei (NeuN), anti-mAChR, and DAPI immunohistochemistry was performed to verify the identity of astrocytes and localization of mAChRs on them. The Student *t* test and Wilcoxon rank-sum test were used for statistical analyses as appropriate. Full details are provided in *SI Materials and Methods*.

ACKNOWLEDGMENTS. We thank K. D. McCarthy (University of North Carolina) for providing the IP_3R2 mice. We thank Michael Goard, Caroline Runyan, Travis Emery, Jonathan Woodson, and Jorge Castro for discussions/technical advice/assistance. This work was supported by an Agency for Science, Technology and Research, Singapore (A*STAR) Fellowship (to N.C.), Marie Curie Fellowship (to G.P.), National Institutes of Health Grants R01EY007023 and R01EY018648 (to M.S.), and a grant from the Simons Foundation (to M.S.).

1. Kitt CA, Höhmann C, Coyle JT, Price DL (1994) Cholinergic innervation of mouse forebrain structures. *J Comp Neurol* 341:117–129.
2. Bakin JS, Weinberger NM (1996) Induction of a physiological memory in the cerebral cortex by stimulation of the nucleus basalis. *Proc Natl Acad Sci USA* 93:11219–11224.
3. Kilgard MP, Merzenich MM (1998) Cortical map reorganization enabled by nucleus basalis activity. *Science* 279:1714–1718.
4. Puckett AC, Pandya PK, Moucha R, Dai W, Kilgard MP (2007) Plasticity in the rat posterior auditory field following nucleus basalis stimulation. *J Neurophysiol* 98:253–265.
5. Bao S, Chang EF, Davis JD, Gobeske KT, Merzenich MM (2003) Progressive degradation and subsequent refinement of acoustic representations in the adult auditory cortex. *J Neurosci* 23:10765–10775.
6. Froemke RC, Merzenich MM, Schreiner CE (2007) A synaptic memory trace for cortical receptive field plasticity. *Nature* 450:425–429.
7. McCormick DA, Prince DA (1986) Mechanisms of action of acetylcholine in the guinea-pig cerebral cortex in vitro. *J Physiol* 375:169–194.
8. Kawaguchi Y (1997) Selective cholinergic modulation of cortical GABAergic cell subtypes. *J Neurophysiol* 78:1743–1747.
9. Xiang Z, Huguenard JR, Prince DA (1998) Cholinergic switching within neocortical inhibitory networks. *Science* 281:985–988.
10. Shelton MK, McCarthy KD (2000) Hippocampal astrocytes exhibit Ca2+-elevating muscarinic cholinergic and histaminergic receptors in situ. *J Neurochem* 74:555–563.
11. Araque A, Martín ED, Perea G, Arellano JI, Buño W (2002) Synaptically released acetylcholine evokes Ca2+ elevations in astrocytes in hippocampal slices. *J Neurosci* 22:2443–2450.
12. Perea G, Araque A (2005) Properties of synaptically evoked astrocyte calcium signal reveal synaptic information processing by astrocytes. *J Neurosci* 25:2192–2203.
13. Yang Y, et al. (2003) Contribution of astrocytes to hippocampal long-term potentiation through release of D-serine. *Proc Natl Acad Sci USA* 100:15194–15199.
14. Perea G, Araque A (2007) Astrocytes potentiate transmitter release at single hippocampal synapses. *Science* 317:1083–1086.
15. Henneberger C, Papouin T, Oliet SHR, Rusakov DA (2010) Long-term potentiation depends on release of D-serine from astrocytes. *Nature* 463:232–236.
16. Agulhon C, Fiacco TA, McCarthy KD (2010) Hippocampal short- and long-term plasticity are not modulated by astrocyte Ca2+ signaling. *Science* 327:1250–1254.
17. Takata N, et al. (2011) Astrocyte calcium signaling transforms cholinergic modulation to cortical plasticity in vivo. *J Neurosci* 31:18155–18165.
18. Navarrete M, et al. (2012) Astrocytes mediate in vivo cholinergic-induced synaptic plasticity. *PLoS Biol* 10:e1001259.
19. Sillito AM, Kemp JA (1983) Cholinergic modulation of the functional organization of the cat visual cortex. *Brain Res* 289:143–155.
20. Murphy PC, Sillito AM (1991) Cholinergic enhancement of direction selectivity in the visual cortex of the cat. *Neuroscience* 40:13–20.
21. Sato H, Hata Y, Masui H, Tsumoto T (1987) A functional role of cholinergic innervation to neurons in the cat visual cortex. *J Neurophysiol* 58:765–780.
22. Zinke W, et al. (2006) Cholinergic modulation of response properties and orientation tuning of neurons in primary visual cortex of anaesthetized Marmoset monkeys. *Eur J Neurosci* 24:314–328.
23. Herrero JL, et al. (2008) Acetylcholine contributes through muscarinic receptors to attentional modulation in V1. *Nature* 454:1110–1114.

24. Goard M, Dan Y (2009) Basal forebrain activation enhances cortical coding of natural scenes. *Nat Neurosci* 12:1444–1449.
25. Dragoi V, Sharma J, Sur M (2000) Adaptation-induced plasticity of orientation tuning in adult visual cortex. *Neuron* 28:287–298.
26. Schummers J, Yu H, Sur M (2008) Tuned responses of astrocytes and their influence on hemodynamic signals in the visual cortex. *Science* 320:1638–1643.
27. Buzsaki G, et al. (1988) Nucleus basalis and thalamic control of neocortical activity in the freely moving rat. *J Neurosci* 8:4007–4026.
28. Runyan CA, et al. (2010) Response features of parvalbumin-expressing interneurons suggest precise roles for subtypes of inhibition in visual cortex. *Neuron* 67:847–857.
29. Nimmerjahn A, Kirchhoff F, Kerr JND, Helmchen F (2004) Sulforhodamine 101 as a specific marker of astroglia in the neocortex in vivo. *Nat Methods* 1:31–37.
30. Araque A, Li N, Doyle RT, Haydon PG (2000) SNARE protein-dependent glutamate release from astrocytes. *J Neurosci* 20:666–673.
31. Bezzi P, et al. (1998) Prostaglandins stimulate calcium-dependent glutamate release in astrocytes. *Nature* 391:281–285.
32. Anderson CM, Swanson RA (2000) Astrocyte glutamate transport: review of properties, regulation, and physiological functions. *Glia* 32:1–14.
33. Di Castro MA, et al. (2011) Local Ca2+ detection and modulation of synaptic release by astrocytes. *Nat Neurosci* 14:1276–1284.
34. Jourdain P, et al. (2007) Glutamate exocytosis from astrocytes controls synaptic strength. *Nat Neurosci* 10:331–339.
35. Hamilton NB, Attwell D (2010) Do astrocytes really exocytose neurotransmitters? *Nat Rev Neurosci* 11:227–238.
36. Fellin T, et al. (2004) Neuronal synchrony mediated by astrocytic glutamate through activation of extrasynaptic NMDA receptors. *Neuron* 43:729–743.
37. Rumbaugh G, Vicini S (1999) Distinct synaptic and extrasynaptic NMDA receptors in developing cerebellar granule neurons. *J Neurosci* 19:10603–10610.
38. Stocca G, Vicini S (1998) Increased contribution of NR2A subunit to synaptic NMDA receptors in developing rat cortical neurons. *J Physiol* 507:13–24.
39. Tovar KR, Westbrook GL (1999) The incorporation of NMDA receptors with a distinct subunit composition at nascent hippocampal synapses in vitro. *J Neurosci* 19: 4180–4188.
40. Shigetomi E, Bowser DN, Sofroniew MV, Khakh BS (2008) Two forms of astrocyte calcium excitability have distinct effects on NMDA receptor-mediated slow inward currents in pyramidal neurons. *J Neurosci* 28:6659–6663.
41. Holtzclaw LA, Pandhit S, Bare DJ, Mignery GA, Russell JT (2002) Astrocytes in adult rat brain express type 2 inositol 1,4,5-trisphosphate receptors. *Glia* 39:69–84.
42. Petravicz J, Fiacco TA, McCarthy KD (2008) Loss of IP3 receptor-dependent Ca2+ increases in hippocampal astrocytes does not affect baseline CA1 pyramidal neuron synaptic activity. *J Neurosci* 28:4967–4973.
43. Zhou Q, Tao HW, Poo MM (2003) Reversal and stabilization of synaptic modifications in a developing visual system. *Science* 300:1953–1957.
44. Jia H, Rochefort NL, Chen X, Konnerth A (2010) Dendritic organization of sensory input to cortical neurons in vivo. *Nature* 464:1307–1312.
45. Somers DC, Nelson SB, Sur M (1995) An emergent model of orientation selectivity in cat visual cortical simple cells. *J Neurosci* 15:5448–5465.
46. Ferster D, Miller KD (2000) Neural mechanisms of orientation selectivity in the visual cortex. *Annu Rev Neurosci* 23:441–471.
47. Schummers J, Sharma J, Sur M (2005) Bottom-up and top-down dynamics in visual cortex. *Progress in Brain Research*, eds Casagrande VA, Guillery RW, Sherman SM (Elsevier, Amsterdam), Vol 149, pp 65–81.
48. Benneyworth M, Li Y, Basu A, Bolshakov V, Coyle J (2012) Cell selective conditional null mutations of serine racemase demonstrate a predominate localization in cortical glutamatergic neurons. *Cell Mol Neurobiol* 32:613–624.
49. Seigneur J, Kroeger D, Nita DA, Amzica F (2006) Cholinergic action on cortical glial cells in vivo. *Cereb Cortex* 16:655–668.
50. Paxinos GFK (2001) *The Mouse Brain in Stereotaxic Coordinates* (Academic, New York).